# Development of an Efficient CFD Model for Nuclear Thermal Thrust Chamber Assembly Design

Gary Cheng*, Yasushi Ito†, Doug Ross‡
*Department of Mechanical Engineering*
*University of Alabama at Birmingham, Birmingham, AL 35294-4461*

Yen-Sen Chen§
*Engineering Sciences, Inc., Huntsville, Alabama, 35815*

Ten-See Wang**
*NASA Marshall Space Flight Center, Huntsville, Alabama, 35812*

***Abstract***

The objective of this effort is to develop an efficient and accurate computational methodology to predict both detailed thermo-fluid environments and global characteristics of the internal ballistics for a hypothetical solid-core nuclear thermal thrust chamber assembly (NTTCA). Several numerical and multi-physics thermo-fluid models, such as real fluid, chemically reacting, turbulence, conjugate heat transfer, porosity, and power generation, were incorporated into an unstructured-grid, pressure-based computational fluid dynamics solver as the underlying computational methodology. The numerical simulations of detailed thermo-fluid environment of a single flow element provide a mechanism to estimate the thermal stress and possible occurrence of the mid-section corrosion of the solid core. In addition, the numerical results of the detailed simulation were employed to fine tune the porosity model mimic the pressure drop and thermal load of the coolant flow through a single flow element. The use of the tuned porosity model enables an efficient simulation of the entire NTTCA system, and evaluating its performance during the design cycle.

## I. Introduction

Nuclear thermal propulsion can carry far larger payloads and reduce travel time for astronauts traveling to Mars and other planets of the solar system than any chemical propulsion currently available. One of the concepts that was extensively tested during the Rover/NERNA era and appear to be the most feasible is the solid-core concept.[1] This concept involves a solid-core reactor consisting of hundreds of heat generating solid flow elements, and each flow element containing tens of flow channels through which the working fluid acquires energy and expands in a high expansion nozzle to generate thrust. Hydrogen is most often chosen as the propellant due to its low molecular weight. The solid-core reactor therefore resembles a heat exchanger. To minimize the effect of its weight, the reactor often operates at very high temperature and power density, which imposes real challenges to the integrity of the flow

* Associate Professor, Senior Member, AIAA. E-mail: gcheng@uab.edu
† Research Assistant Professor, Member AIAA
‡ Programmer
§ President, Member AIAA
** Technical Assistant, ER43, Thermal and Combustion Analysis Branch, Senior Member AIAA

element material. To make the solid-core reactor a viable concept for Mars missions, we must understand the effect of hydrogen as a high temperature working fluid and develop materials that withstand the harsh flow element environment.

One of the impacts of operating at the combination of high temperature and high power density is a phenomenon known as the mid-section corrosion, as reported during the legacy engine tests.[1, 2] There was an excessive mass loss of the flow element material near the mid-section during testing. The symptom was cracked coating layer while the purpose of coating was to isolate the carbonaceous compound in the flow element matrix from the attack by hydrogen. The causes of mid-section corrosion were speculated as a mismatch in the thermal expansion of flow element and its coating material, large temperature gradients in the solid core, and change of solid thermal property due to irradiation.[4] Note that another speculation was that the flow was choked in the long flow channels of the flow element.

One way to help understanding the effect of hydrogen as a working fluid and developing materials that withstand the harsh environment is to develop computational methodology that can accurately predict thermo-fluid environments inside the nuclear thermal thrust chamber assembly and reproduce the flow element thermal environment occurring in the legacy engine tests. The objective of this effort is therefore to develop an efficient and accurate multiphysics thermal-fluid computational methodology to predict environments for a hypothetical solid-core thrust chamber and the associated flow element, similar to those in the Small Engine.[1] The Small Engine was a paper engine designed near the end of the Rover/NERVA era and bears common features of other legacy engines tested during that time period, but was never built nor tested. The hypothetical thrust chamber and flow element, which are being redesigned by the System Analysis Group at Marshall Space Flight Center, consists of 564 flow elements and of 19 flow channels for each flow element, respectively. The computational methodology was based on an existing Unstructured-grid Navier-Stokes Internal-external computational fluid dynamics Code (UNIC[5-7]). Conjugate heat transfer formulations for coupling fluid dynamics and conductive heat transfer in solids and for flow and conductive heat transfer in porous media were developed and tested. The UNIC code has been well validated and employed to simulate a great variety of engineering problems ranging from internal to external flows, incompressible to compressible flows, single-phase to multi-phase flow, and inert to reacting flows.

Figure1: Geometry of a 19-channel flow element

A two-pronged approach was employed in this effort: a detailed analysis of a NERVA-type 19-channel flow element, and a global analysis of the entire thrust chamber. Two groups of detailed analyses were conducted for the 19-channel flow element, as shown in Figure 1. The first group simulated the full-length 19-channel flow element with three different power generation distributions to investigate the occurrence of mid-section corrosion problem and potential flow chocking in the flow channel. These three distributions include pure sine function in the axial direction with pure cosine function in the radial direction, pure sine function in the axial direction with clipped cosine function in the radial direction, and clipped sine function in the axial direction with clipped cosine function in the radial

direction. The second group simulated a one-eighth-length 19-channel flow element with different side-wall temperature and flow channel diameters to obtain data for calibrating the porosity model used in the global analysis of the entire thrust chamber. In the global thrust chamber analysis, the 19-channels for each flow element were lumped together as a porous media to save computational resources, and the core surrounding components such as the slats and reflector were treated as heat conducting solids to provide accurate boundary condition for the solid-core environment. The porosity model is employed to represent the effect of the friction loss and heat transfer as the working fluid flowing through the flow element. The use of the porosity model enables an efficient simulation of the entire thrust chamber, and evaluation of its performance during the design cycle.

In order to support both the detailed and global analyses, several physical submodels were either improved or added into the UNIC code[8-9]. These code improvements include: an anisotropic drag and heat transfer porosity model to account for the directional effect of the flow channel, a source term in the energy to model the power generation of the solid core with a user's specified distributions, validation of the conjugate heat transfer capability built in the UNIC code with a well known thermal analysis code, SINDA[10] to provide an accurate calculation of heat transfer through the solid-fluid interface. The tuned porosity model for the flow element and the numerical results of both the detailed and global analyses are reported herein. .

## II. Numerical Methodology

### A. Computational Fluid Dynamics

The employed CFD solver, UNIC, solves a set of Reynolds-averaged governing equations (continuity, Navier-Stokes, energy, species mass fraction, etc.) to satisfy the conservation laws for a turbulent flow of interest. The set of governing equation can be written in Cartesian tensor form:

$$\frac{\partial \rho}{\partial t}+\frac{\partial}{\partial x_j}(\rho V_j)=0 \tag{1}$$

$$\frac{\partial(\rho V_i)}{\partial t}+\frac{\partial}{\partial x_j}(\rho V_j V_i)=-\frac{\partial p}{\partial x_i}+\frac{\partial(\tau_{ji}+\tau_t)}{\partial x_j}+S_V \tag{2}$$

$$\frac{\partial(\rho h_t)}{\partial t}+\frac{\partial}{\partial x_j}(\rho V_j h_t)=\frac{\partial p}{\partial t}+\frac{\partial}{\partial x_j}\left[\left(\frac{\mu}{\mathrm{Pr}}+\frac{\mu_t}{\mathrm{Pr}_t}\right)\frac{\partial h}{\partial x_j}\right]+\frac{\partial V_i(\tau_{ji}+\tau_t)}{\partial x_j}+Q_r+S_h \tag{3}$$

$$\frac{\partial(\rho k)}{\partial t}+\frac{\partial}{\partial x_j}(\rho V_j k)=\frac{\partial}{\partial x_j}\left[\left(\mu+\frac{\mu_t}{\sigma_k}\right)\frac{\partial k}{\partial x_j}\right]+\rho(\Pi-\varepsilon) \tag{4}$$

$$\frac{\partial(\rho \varepsilon)}{\partial t}+\frac{\partial}{\partial x_j}(\rho V_j \varepsilon)=\frac{\partial}{\partial x_j}\left[\left(\mu+\frac{\mu_t}{\sigma_\varepsilon}\right)\frac{\partial \phi}{\partial x_j}\right]+\rho\frac{\varepsilon}{k}\left(C_1\Pi-C_2\varepsilon+C_3\frac{\Pi^2}{\varepsilon}\right) \tag{5}$$

$$\frac{\partial(\rho \alpha_i)}{\partial t}+\frac{\partial}{\partial x_j}(\rho V_j \alpha_i)=\frac{\partial}{\partial x_j}\left[\left(\frac{\mu}{Sc}+\frac{\mu_t}{Sc_t}\right)\frac{\partial \alpha_i}{\partial x_j}\right]+S_i \tag{6}$$

where $\rho$ is the fluid density $p$ is the pressure, $V_j = (u, v, w)$ stands for the velocity components in $x$-, $y$-, and $z$-coordinates respectively, $h_t$ and $h$ are the total and static enthalpies, $k$ is the turbulence kinetic energy, $\Pi$ and $\varepsilon$ are the production and dissipation rates of turbulence, $\alpha_i$ and $S_i$ are the mass fraction and production/destruction rate of $i$-th species, $Q_r$ is the radiative heat flux, $S_V$ and $S_h$ are the source/sink terms of the momentum and energy equations, $\mu$ and $\mu_t$ are the fluid and eddy viscosity, $\tau_{ji}$ and $\tau_t$ are the viscous stress and Reynolds stress, Pr and $\mathrm{Pr}_t$ are the Prandtl and turbulent Prandtl numbers, $Sc$ and $Sc_t$ are Schmidt and turbulent Schmidt numbers, $C_1$, $C_2$, $C_3$, $\sigma_k$, and $\sigma_\varepsilon$ are turbulence modeling constants. Detailed expressions for the $k$-$\varepsilon$ models and wall functions can be found in [11]. An extended $k$-$\varepsilon$ turbulence model[12] was used to close the system of Reynolds-averaged governing equations. A modified wall function approach[13, 14] was employed to provide wall boundary layer solutions that are less sensitive to the near-wall grid spacing.

A predictor and multi-corrector pressure-based solution algorithm[15, 16] was employed in the UNIC code to couple the set of governing equations such that both compressible and incompressible flows can be solved in a unified framework without using ad-hoc artificial compressibility and/or a pre-conditioning method. The employed predictor-corrector solution method[5] is based on modified pressure-velocity coupling approach of the SIMPLE-type[16] algorithm which includes the compressibility effects and is applicable to flows at all speeds. In order to handle problems with complex geometries, the UNIC code employs a cell-centered unstructured finite volume method[6, 7] to solve for the governing equations in the curvilinear coordinates, in which the primary variables are the Cartesian velocity components, pressure, total enthalpy, turbulence kinetic energy, turbulence dissipation and mass fractions of chemical species.

The inviscid flux is evaluated through the values at the upwind cell and a linear reconstruction procedure to achieve second order accuracy. A multi-dimensional linear reconstruction approach by Barth and Jespersen[17] was used in the cell reconstruction to achieve higher-order accuracy for the convection terms. A second-order central-difference scheme was employed to discretize the diffusion fluxes and source terms. A dual-time sub-iteration method is employed for time-accurate time-marching computations. A pressure damping term, Rhie and Chow[18], is applied to the evaluation of mass flux at the cell interface to avoid the even-odd decoupling of velocity and pressure fields. All the discretized governing equations are solved using the preconditioned Bi-CGSTAB[19] matrix solver, except the pressure-correction equation which has an option to be solved using GMRES[20] matrix solver when the matrix is ill-conditioned. An algebraic multi-grid (AMG) solver[21] was included such that users can activate to improve the convergence if desired. The UNIC code also has mesh refinement and coarsening capabilities to improve the numerical accuracy and computational efficiency. In order to efficiently simulate problems involving large numbers of meshes, the UNIC code employed parallel computing with domain decomposition, where exchange of data between processors is done by using MPI[22]. Domain decomposition (partitioning the computational domain into several sub-domains handled by different computer processors) can be accomplished by using METIS[23] or a native partitioning routine in the UNIC code.

In addition, numerous submodels were incorporated in the UNIC code to model various physics and transport phenomena. These submodels include: 1) finite-rate and equilibrium chemistry for combustion, 2) conjugate heat transfer for coupling heat convection and conduction, 3) both the heterogeneous spray model with Eulerian/Lagrangian approach and the homogeneous spray model with the Eulerian/Eulerian approach and real-fluid property models

for liquid spray flow, 4) the finite volume method for solving radiation transport equation (RTE), 5) solving translational and vibrational energy equations for thermal non-equilibrium effect, 6) porosity model for flow through a porous media, etc. During the last decade, the UNIC code has been improved to equip models appropriate to resolve the complex physics, and has been employed to simulate a great variety of engineering problems. The results have shown that the UNIC code is as computationally efficient as any CFD codes. Hence, we employed the UNIC code and modified it to account for some specific effects of interest in the present study, such as power generation, non-isotropic porosity with or without heat conduction, variable thermal conductivities and specific heat based on different solid materials and temperatures. Some of these code improvements performed in this study are described in the following.

**B. Conjugate Heat Transfer:**

The framework of conjugate heat transfer is to solve the heat transfer in the fluid flow and the heat conduction in the solid in a coupled manner. The governing equation describing the heat transfer in the fluid flow is shown in Eq. (3), where the heat conduction in the solid can be written as:

$$\frac{\partial \rho C_p T}{\partial t} - \frac{\partial}{\partial x_i}\left(\kappa \frac{\partial T}{\partial x_i}\right) = Q_v + \frac{\partial Q_s}{\partial x_i} \tag{7}$$

where $Q_v$ and $Q_s$ represent source terms from volumetric and boundary contributions, respectively. $\kappa$ and $C_p$ denote the thermal conductivity and capacity of the solid material, respectively. In the case of simulating solid core with power generation, $Q_v$ depends on power generation distributions function employed. In the present study, three power distribution functions were examined: (i) pure sine function in the axial direction with pure cosine function in the radial direction; (ii) pure sine function in the axial direction with clipped cosine function in the radial direction; (iii) Clipped sine function in the axial direction with clipped cosine function in the radial direction. The temperature value at the fluid-solid interface is obtained by enforcing the heat flux continuity condition, i.e. $Q_s = -q_w$ where $q_w$ is the heat flux from the fluid to the solid calculated by solving Eq. (3) including the turbulence effect if applicable. In order to achieve numerical stability and enforce the heat flux continuity condition, an implicit treatment of the temperature at the fluid-solid interface is employed. In this approach, Eq. (7) can be discretized as

$$\frac{1}{2}\rho C_p \frac{T_b^{n+1} - T_b^n}{\Delta t} = \frac{1}{\Delta y_n}\left(k \frac{T_c^n - T_b^n}{\Delta y_n} - q_w\right) \tag{8}$$

where the superscripts $n$+1 and $n$ denote the values at the next and current time levels, respectively. $T_b$ and $T_c$ are the temperatures at the fluid-solid interface and at the center of the solid cell next to the fluid-solid interface in respect. $y_n$ represents the normal distance from the interface to the center of the solid cell next to the fluid-solid interface. The ½ factor on the left hand side of the above equation is because only half of the solid cell is involved in the control volume. It can be seen that this scheme can be applied to both transient and steady state simulations. For steady-state simulations, an acceleration factor can be used to improve convergence of heat conduction in the solid. Implementation of the implicit treatment has been validated[9] by comparing with the SINDA code.

**C. Porosity Model:**

In the present study, a porosity model was developed to represent the momentum and energy transport through an assembly of flow pipes, and the heat conduction through the solid material within a flow element. Hence, the porosity model will include separate temperatures and thermal conductivities for both the solid material and fluid flow. The momentum and energy equations for the fluid flow are the same as Eqs. 2 & 3, except the source terms will be modified to account for the extra friction loss and heat transfer. The source term of the momentum equation (Eq. 2) can be expressed as

$$\vec{S}_V = \frac{D}{\xi \forall} = \frac{1}{2}\frac{\rho |V_s| C_f}{\xi^2 d/4}\vec{V}_s \tag{9}$$

where $D$ is the drag force modeled by the porosity model, $\xi$ is the porosity factor for the porous region, $V_s$ is the superficial flow velocity through the porous region, $d$ is diameter of the flow channel, and $\forall$ is the total volume of the porous region. An empirical correlation of the friction coefficient ($C_f$) for the flow through a pipe, known as the Blasius formula[24], is used and expressed as follow.

$$C_f = 0.0791 \mathrm{Re}_d^{-0.25} \quad \text{where} \quad \mathrm{Re}_d = \frac{\rho V_s d}{\mu \xi}$$

The source term for the energy equation (Eq. 3) can be calculated as

$$S_h = \frac{Q}{\xi \forall} = \frac{f}{2}\frac{\rho |V_s| C_f}{\mathrm{Pr}^{2/3} \xi d/4} C_p \Delta T \quad \text{where} \quad \Delta T = T_s - T_g \tag{10}$$

where $Q$ is the heat sink/source due to the fluid-solid interaction in the porous region, Pr is the Prandtl number of the fluid, $f$ is an empirical parameter will be tuned by comparing solutions of the porosity model and the detailed conjugate heat transfer model, and $T_s$ and $T_g$ are the temperatures of the solid and fluid at the same location, respectively. In addition, the source term of the heat conduction equation (Eq. 7) in the porous region can be calculated as

$$Q_v = \frac{Q}{(1-\xi)\forall} = \frac{f}{2}\frac{\rho |V_s| C_f}{\mathrm{Pr}^{2/3}(1-\xi) d/4} C_p \Delta T \quad \text{and} \quad \Delta T = T_g - T_s \tag{11}$$

while $Q_s = 0$.

## III. Numerical Meshes

For the numerical simulations with the conjugate heat transfer model, two mesh systems need to be constructed. One of them is employed to model the entire computational domain including both the solid grain and the flow channel. The other one is used by the code to identify the region of solid material, and thus it can be very coarse. Hence, there is no need for a special grid generator to construct multi-block meshes for separating the solid and the fluid region, neither the identification for the fluid-solid interface. In the present study, various flow element geometries were simulated, such as different flow channel diameter, with and without coating layer in the solid core, and different flow channel length. Hence, a geometry/grid template, as shown in Figure 2, was developed based on MiniCAD[25-27] to expedite the geometry and grid generation process by allowing the user to interactively change 1) the ratio of the gap between flow channels to the diameter of flow channel, 2) the ratio of the size of the flow element to the diameter of the flow channel, 3) thickness of the coating layer, and 4) the length of the flow element. The benefit of using MiniCAD is the ability to have graphical feedback while building the geometry and grid, and to easily move dimensional values from the geometry into the

template to make it easy to create grids with modified values. In the present study, a 60° pi-section of a single flow element, which includes 3 and 1/6 flow channels, was simulated.

MiniCAD is a graphical user interface (GUI) built on the Geometry Grid Toolkit (GGTK). The geometry that defines the dimensions of the solid grain was also exported in the stereolithography (STL) format, which can be used by an in-house grid generator to construct the hybrid mesh for the entire flow element. The process of building grid in MiniCAD involves three basic steps. Step one is to create or import the geometry. Step two is to pass the geometry to a grid topology to ensure that the mesh built will be geometrically watertight. Step 3 is to build the mesh based on the grid topology. Based on our investigation, we found the most efficient structured grid topology to model the solid grain is an O-type grid. In this case, the solid grain was decomposed into multiple blocks (5 blocks for cases without coating layer, and 10 blocks for those with coating layer), where the O-grids of each block were used to model the solid grain and coating layer (if present) surrounding each flow channel as shown in Figure 2. A separate block is needed to identify the coating layer because it has different thermal properties from those of the solid grain. The boundary of the O-grid geometry for each flow channel was built as a planar trimmed surface. This geometry was converted to the topology structure and then a 2-D grid was built on the faces. Since the grid for the solid grain is only used to identify the region of solid grain and is geometrically similar in the axial direction, it was only necessary to create the 3-D grid by extruding the 2-D grid in the axial direction, which can be seen in Figure 3.

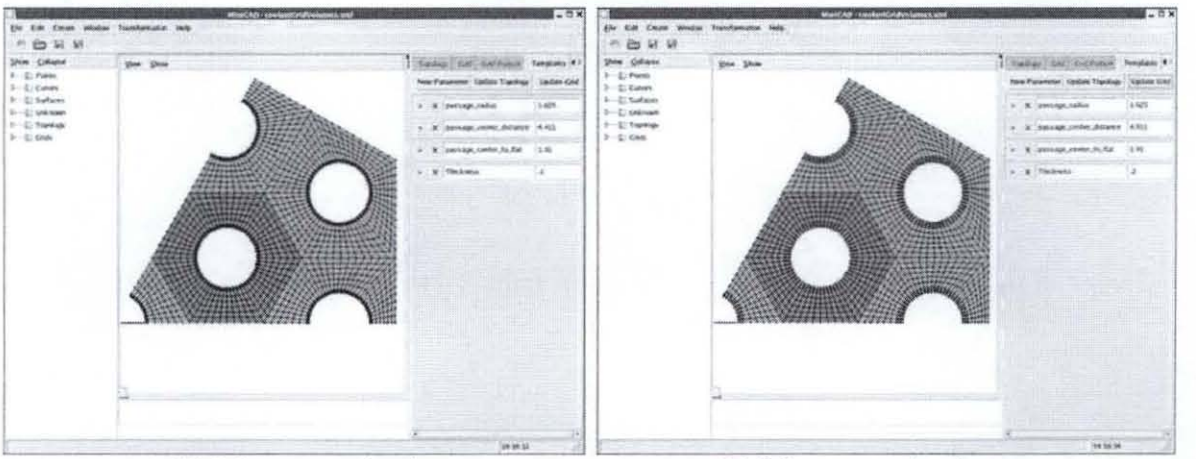

(a) 0.1 mm coating layer (b) 0.2 mm coating layer

Figure 2: Layout of the developed geometry/grid template (flow channel diameter = 2.05 mm)

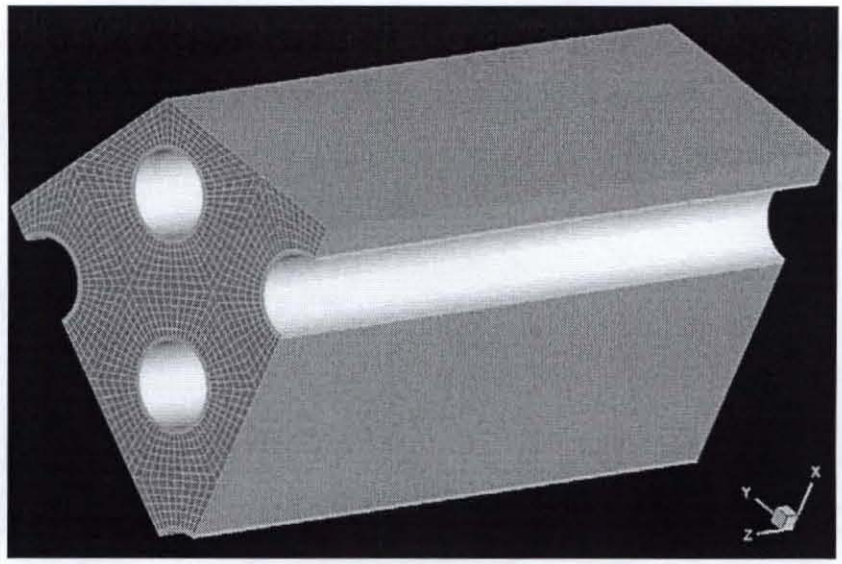


Figure 3: Structured grid system for the solid grain and coating layer of a flow element

To accurately resolve the momentum and energy transport near the solid-fluid interface, a hybrid mesh topology was employed to generate the mesh for the entire flow element. The procedure used by our in-house grid generator is to construct the surface mesh before creating the 3-D volume mesh. For surface mesh generation, a direct advancing front method is used [28, 29]. A discrete model in STL format, imported from MiniCAD, is used as a background mesh, on which a new surface mesh suitable for computational simulations is created. Geometrical features are extracted based on a folding angle at each edge. A user specifies node distributions on the geometrical features, which form an initial front for the advancing front method. The surface triangulation is performed in the physical 3D space in order to check the quality of triangles easily.

For volume mesh generation, two approaches were used. One is a method to create regular hybrid meshes based on an advancing layer method. In this method, a multiple marching direction approach is employed to create better control volumes around sharp convex corners [30]. Figure 4 shows a hybrid mesh inside a flow element, which has 335,207 nodes, 688,027 tetrahedra, 21,476 prisms, 33,655 pyramids and 167,259 hexahedra. Quadrangles are used for the pipe surfaces. Multiple marching directions are defined at pipe inlets, which enable smooth transition of the mesh size there.

The other volume mesh generation method is an extrusion method based on a 2-D mesh to create volume meshes more easily. Every cross-section across the symmetry axis is the same. First, a 2-D mesh is created as shown in Figure 5. Second, it is extruded toward the symmetry axis, following the user-specified spacing. Third, boundary surfaces are numbered so that boundary conditions are set for CFD simulations.

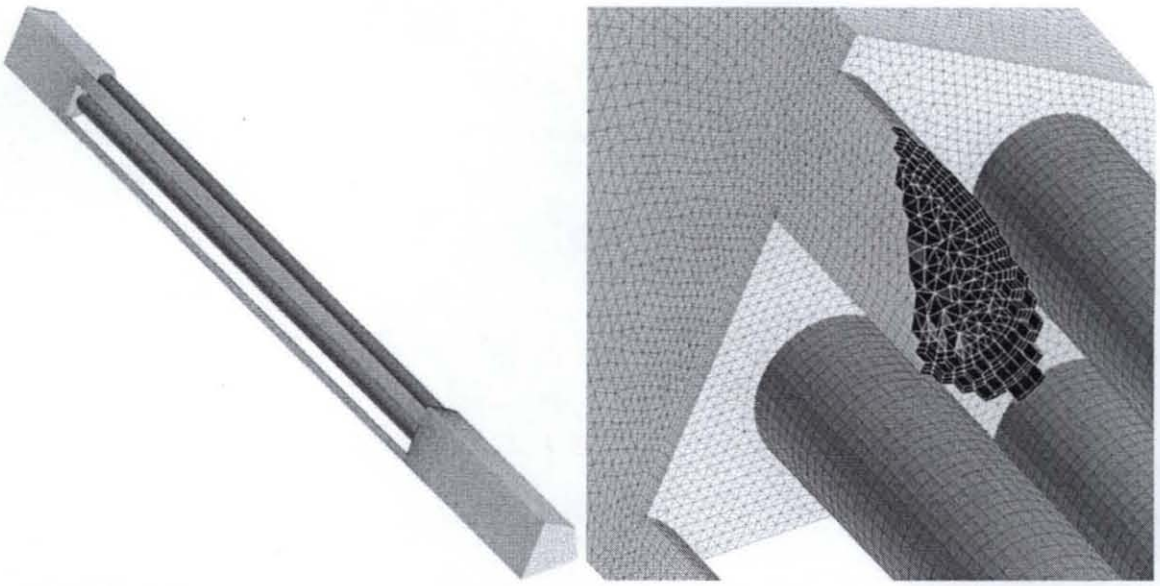

**Figure** 4: Regular hybrid meshes: (a) surface mesh; (b) cross-section of hybrid volume mesh

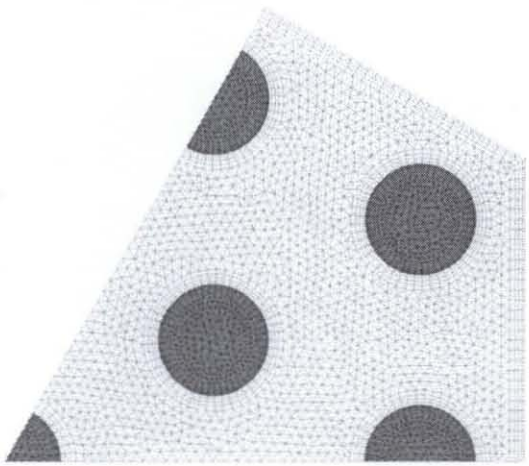

**Figure** 5: 2D mesh for the extrusion method: solid part (yellow) and fluid part (green)

## IV. Results and Discussion

The numerical results will be presented and discussed in the full length paper


## Acknowledgments

This study was partially supported by a Nuclear Systems Office task entitled "Multiphysics Thrust Chamber Modeling" of which Wayne Bordelon was the project manager. Steve Simpson and Karl Nelson provided nozzle geometry and operating conditions for the hypothetical nuclear thermal engine. Bill Emrich suggested the Cosine power profile. Thermal properties provided by Panda Binayak, Robert Hickman, and Bill Emrich are also acknowledged.

## References


1. Koenig, D.R., "Experience Gained from the Space Nuclear Rocket Program (Rover)," LA-10062-H, Los Alamos National Laboratory, Los Alamos, New Mexico, 1986.
2. Lyon, L.L., "Performance of (U, Zr)C-Graphite (Composite) and of (U, Zr)C (Carbide) Fuel Elements in the Nuclear Furnace 1 Test Reactor," LA-5398-MS, Los Alamos Scientific Laboratory, Los Alamos, New Mexico, 1973.
3. Wang, T.-S., Luong, V., Foote, J., Litchford, R., and Chen, Y.-S., "Analysis of a Cylindrical Specimen Heated by an Impinging Hot Hydrogen Jet," AIAA Paper 2006-2926, 9th AIAA/ASME Joint Thermophysics and Heat Transfer Conference, San Francisco, CA, 2006.
4. Chen, Y.-S., Liu, J., Zhang, S., and Mallapragada, P., "An Integrated Tool for Launch Vehicle Base-Heating Analysis," Final Report, NAS8-00002, Engineering Sciences, Inc., Huntsville, AL, 2001.
5. Chen, Y.S., "An Unstructured Finite Volume Method for Viscous Flow Computations", 7th International Conference on Finite Element Methods in Flow Problems, University of Alabama in Huntsville, Huntsville, Alabama, Feb. 3-7, 1989.
6. Shang, H.M., Shih, M.H., Chen, Y.S., and Liaw, P., "Flow Calculation on Unstructured Grids with a Pressure-Based Method," Proceedings of 6th International Symposium on Computational Fluid Dynamics, Lake Tahoe, NV, Sep. 4-8, 1995.
7. Chen. Y.-S., Zhang S., and Liu, J., "Stage Separation Performance Analysis Project," Final Report, H-34345D, Engineering Sciences, Inc., Huntsville, AL, 2002.
8. Wang, T.S., Canabal, F., Cheng, G.C., and Chen, Y.S., "Multiphysics Analysis of a Solid-Core Nuclear Thermal Engine Thrust Chamber," AIAA Paper 2006-2927, 9th AIAA/ASME Joint Thermophysics and Heat Transfer Conference, June 5-8, 2006.
9. Wang, T.S., Luong, V., Foote, J., and Chen, Y.S., "Analysis of a Cylindrical Specimen Heated by an Impinging Hot Hydrogen Jet," AIAA Paper 2006-2926, 9th AIAA/ASME Joint Thermophysics and Heat Transfer Conference, June 5-8, 2006.
10. Gaski, J., "The Systems Improved Numerical Differencing Analyzer (SINDA) Code – a User's Manual," Aerospace Corp., El Segundo, CA, Feb. 1986
11. Launder, B.E. and Spalding, D.B., "The Numerical Calculation of Turbulent Flows," *Computer Methods in Applied Mechanics and Engineering*, Vol. 3(2), pp. 269-289, 1974.
12. Chen, Y.-S., and Kim, S. W., "Computation of Turbulent Flows Using an Extended k-ε Turbulence Closure Model," NASA CR-179204, 1987.
13. Liakopoulos, A., "Explicit Representations of the Complete Velocity Profile in a Turbulent Boundary Layer," *AIAA Journal*, Vol. 22, No. 6, June 1984, pp. 844-846.
14. Viegas, J.R., Rubesin, M.W., and Horstman, C.C., "On the Use of Wall Function as Boundary Conditions for Two-Dimensional Separated Compressible Flows," AIAA Paper 85-0180, AIAA 23rd Aerospace Sciences Meeting, Jan. 14-17, 1985.
15. Karki, K.C., and Patankar, S.V., "Pressure Based Calculation Procedure for Viscous Flows at all Speeds in Arbitrary Configurations," AIAA J., Vol. 27, pp. 1167-1174, 1989.
16. Patankar, S.V., *Numerical Heat Transfer and Fluid Flow*, Hemisphere, New York, 1980.
17. Barth, T.J., and Jespersen, D.C., "The Design and Application of Upwind Schemes on Unstructured Meshes," AIAA Paper 89-0366, 1989.
18. Rhie, C.M. and Chow, W.L., "A Numerical Study of the Turbulent Flow past an Isolated Airfoil with Trailing Edge Separation," *AIAA Journal*, Vol. 21, pp. 1525-1532, 1983.

19. Van Der Vorst, H.A., "Bi-CGSTAB: A Fast and Smoothly Converging Variant of Bi-CG for the Solution of Nonsymmetric Linear Systems," *SIAM J. Sci. Stat. Comput.*, Vol. 13(2), pp. 631-644, 1992.
20. Saad,Y. and Schultz, M.H., "GMRES: A Generalized Minimal Residual Algorithm for Solving Nonsymmetric Linear Systems," *SIAM J. Sci. Stat. Comput.*, Vol. 7(3), pp. 856-869, 1986.
21. Raw, M., "Robustness of Coupled Algebric Multigrid for the Navier-Stkoes Equations," AIAA Paper 96-0297, 1996.
22. W. Gropp, E. Lusk, and A. Skjellum, "*Using MPI*", published by MIT Press, ISBN 0-262-57104-8.
23. Karypis and V. Kumar, "METIS, A Software Package for Partitioning Unstructured Graphs, Partitioning Meshes, and Computing Fill-Reducing Orderings of Sparse Matrices," Version 3.0.3, November 5, 1997.
24. Bird, R.B., Stewart, W.E., and Lightfoot, E.N., "*Transport Phenomena*," 2nd Ed., John Wiley & Sons, Inc.
25. Ross, D.H., Dillavou, M., Gopalsamy, S., Shum, P.C., and Shih, A.M., "A Framework for Developing Geometry-Grid Templates for Propulsion Elements," the 16th NASA Thermal and Fluids Analysis Workshop, Orlando, FL, August 8-12, 2005.
26. Shih, A. M., Gopalsamy, S., Ito, Y., Ross, D. H., Dillavou, M. and Soni, B. K., "Automatic and Parametric Mesh Generation Approach," 17th International Association for Mathematics and Computers in Simulation (IMACS) World Congress, Paris, France, July 2005.
27. Shih, A.M., Ross, D.H., Dillavou, M., Gopalsamy, S., Soni, B.K., Peugeot, J.W., and Griffin, L.W., "A Geometry-Grid Generation Template Framework for Propellant Delivery System," 42nd AIAA/ASME/SAE/ASEE Joint Propulsion Conference and Exhibit, Sacramento, CA, July, 2006.
28. Ito, Y. and Nakahashi, K., "Direct Surface Triangulation Using Stereolithography Data," *AIAA Journal*, Vol. 40, No. 3, March 2002, pp. 490-496.
29. Ito, Y. and Nakahashi, K., "Surface Triangulation for Polygonal Models Based on CAD Data," *International Journal for Numerical Methods in Fluids*, Vol. 39, Issue 1, May 2002, pp. 75-96.
30. Ito, Y., Shih, A. M., Soni, B. K. and Nakahashi, K., "An Approach to Generate High Quality Unstructured Hybrid Meshes," AIAA Paper 2006-0530, 44th AIAA Aerospace Sciences Meeting and Exhibit, Reno, NV, January 2006.